

The nature of the embedded intermediate-mass T Tauri star DK Cha[★]

Rebeca Garcia Lopez^{1,2,3}, Brunella Nisini², Simone Antonucci², Alessio Caratti o Garatti¹, Dario Lorenzetti², Teresa Giannini², Jochen Eisloffel⁴, and Tom Ray¹

¹ Dublin Institute for Advanced Studies, School of Cosmic Physics, 31 Fitzwilliam Place, Dublin 2, Ireland

² INAF-Osservatorio Astronomico di Roma, Via di Frascati 33, I-00040 Monteporzio Catone, Italy

³ Max-Planck-Institut für Radioastronomie, Auf dem Hügel 69, D-53121 Bonn, Germany

⁴ Thüringer Landessternwarte Tautenburg, Sternwarte 5, 07778 Tautenburg, Germany

Received date; Accepted date

ABSTRACT

Context. Most of our knowledge about star formation is based on studies of low-mass stars, whereas very little is known about the properties of the circumstellar material around young and embedded intermediate-mass T Tauri stars (IMTTS) mostly because they are rare, typically more distant than their lower mass counterparts, and their nearby circumstellar surroundings are usually hidden from us.

Aims. We present an analysis of the excitation and accretion properties of the young IMTTS DK Cha. The nearly face-on configuration of this source allows us to have direct access to the star-disk system through the excavated envelope and outflow cavity.

Methods. Based on low-resolution optical and infrared spectroscopy obtained with SofI and EFOSC2 on the NTT we derive the spectrum of DK Cha from $\sim 0.6\mu\text{m}$ to $\sim 2.5\mu\text{m}$. From the detected lines we probe the conditions of the gas that emits the H_I IR emission lines and obtain insights into the origin of the other permitted emission lines. In addition, we derive the mass accretion rate (\dot{M}_{acc}) from the relationships that connect the luminosity of the Br γ and Pa β lines with the accretion luminosity (L_{acc}).

Results. The observed optical/IR spectrum is extremely rich in forbidden and permitted atomic and molecular emission lines, which makes this source similar to very active low-mass T Tauri stars. Some of the permitted emission lines are identified as being excited by fluorescence. We derive Brackett decrements and compare them with different excitation mechanisms. The Pa β /Br γ ratio is consistent with optically thick emission in LTE at a temperature of ~ 3500 K, originated from a compact region of $\sim 5 R_{\odot}$ in size: but the line opacity decreases in the Br lines for high quantum numbers n_{up} . A good fit to the data is obtained assuming an expanding gas in LTE, with an electron density at the wind base of $\sim 10^{13} \text{ cm}^{-3}$. In addition, we find that the observed Brackett ratios are very similar to those reported in previous studies of low-mass CTTSs and Class I sources, indicating that these ratios are not dependent on masses and ages. Finally, $L_{acc} \sim 9L_{\odot}$ and $\dot{M}_{acc} \sim 3 \times 10^{-7} M_{\odot} \text{ yr}^{-1}$ values were found. When comparing the derived \dot{M}_{acc} value with that found in Class I and IMTTSs of roughly the same mass, we found that \dot{M}_{acc} in DK Cha is lower than that found in Class I sources but higher than that found in IMTTSs. This agrees with DK Cha being in an evolutionary transition phase between a Class I and II source.

Key words. stars: formation – stars:circumstellar matter – stars: pre-main sequence – ISM:individual objects: DK Cha, IRAS 12496-7650 – Infrared: ISM

1. Introduction

Intermediate-mass T Tauri stars are the young precursors of Herbig AeBe stars with spectral types ranging from K to late F, and ranging from $1 M_{\odot}$ to $5 M_{\odot}$ (e.g. Calvet et al. 2004). Their disks dissipate in ~ 5 Myr, i.e., more quickly than their low-mass classical T Tauri (CTT) counterparts, which makes it very difficult to study them in the early evolutionary phase. Besides, the complex structure of the emission region surrounding protostars makes it more difficult to probe the disk accretion properties, a crucial step towards understanding disk evolution in intermediate-mass stars.

In the nearby surroundings of protostars one does indeed expect emission from the heated dense envelope, the disk, the jet and the UV-heated and shocked cavity walls, excavated by the outflow. Information about the different phenomena involv-

ing the emission from each of the components of this system can only be probed through spectroscopic studies that allow us to obtain quantitative information on processes that take place in spatially unresolved regions (such as the accretion through funnel flows and the ejection of matter from the inner disk). For instance, the jet properties can be studied through forbidden emission lines, while the accretion properties are usually probed through H_I transitions. In this context, infrared spectroscopy turns out to be a very useful tool to study embedded YSOs where the high extinction usually prevents us from observing them through the standard optical tracers. However, in a small number of cases, when the object is observed face-on, we can have direct access to the star-disk system through the outflow cavity and excavated envelope even at shorter wavelengths.

The IMTTS DK Cha ($M_{*}=2 M_{\odot}$, $L_{bol}=29.4L_{\odot}$) is one of these rare examples where, thanks to its nearly face-on configuration ($i \lesssim 18^{\circ}$), the star-disk system can be studied through optical/infrared tracers (van Kempen et al. 2009, 2010; Spezzi et al. 2008; Hughes et al. 1991). DK Cha has been identified as a young object still surrounded by its envelope, as shown by the large amount of warm molecular gas detected on-source and

Send offprint requests to: R. Garcia Lopez, e-mail: rgarcia@mpifr.de

[★] Based on observations collected at the European Southern Observatory, La Silla and Paranal, Chile (ESO program 082.C-0264(A) and 084.C-0308(A)).

ChaII - DK Cha

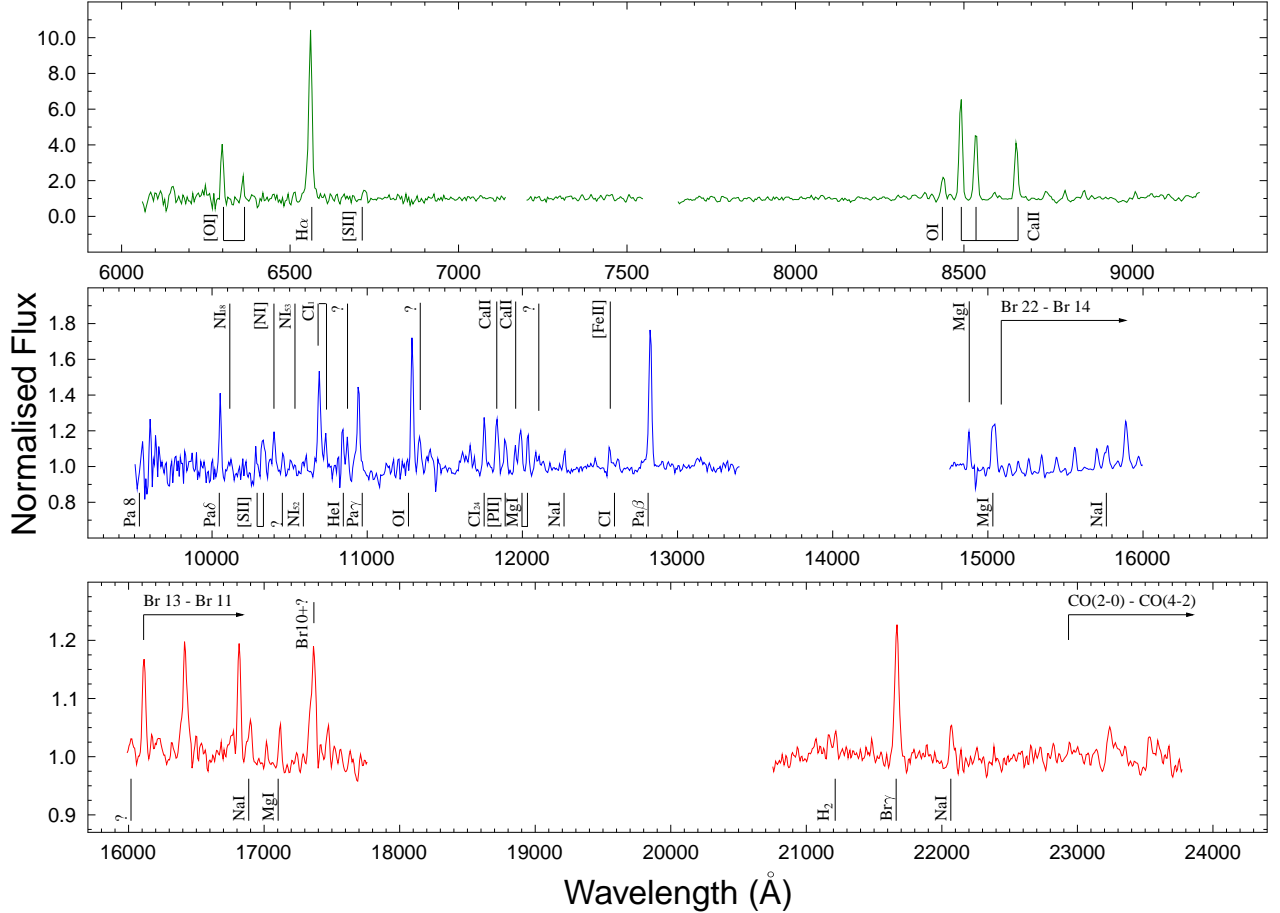


Fig. 1. Normalised to the continuum EFOSC2+SofI spectra from 0.6 to 2.4 μm of the PMS star DK Cha. The strongest lines are identified.

the presence of a strong molecular outflow (van Kempen et al. 2009, 2006). In addition, its spectral energy distribution (SED) corresponds to that of an YSO in a transition phase from a Class I to a Class II source (van Kempen et al. 2010; Spezzi et al. 2008). These characteristics together with its nearby location ($d \sim 178$ pc) make DK Cha an ideal candidate to probe the first stages of the formation of Herbig Ae stars.

Most of our knowledge about this source is based on far-IR and sub-millimeter observations (e.g., van Kempen et al. 2006, 2010; Giannini et al. 1999). Optical spectroscopic studies of DK Cha have been made by Hughes et al. (1991). In that work the first extensive study of the optical and infrared photometric variability of DK Cha was also reported, pointing out the highly variable nature of this source. Here, we will present an optical/IR spectroscopic study of DK Cha aimed at obtaining insights into the characteristics of its circumstellar material and accretion properties. This study was conducted as part of the POISSON (Protostellar Objects IR-optical Spectral Survey On NTT) project, whose results will be presented in a series of papers on the properties of YSOs belonging to different clouds (e.g. ChaI-II regions and L1641 Antoniucci et al. 2011; Caratti o Garatti et al. 2011).

In Sect. 2 the observations and the data reduction will be described, while in Sect. 3 the first complete spectrum of DK Cha from 0.6 to 2.4 μm will be presented. In Sect. 4 we show the

analysis and discuss our observations. Finally, we present the conclusions in Sect. 5.

2. Observations and data reduction

As part of the POISSON project, we observed DK Cha in the wavelength range from $\sim 0.6 \mu\text{m}$ to $\sim 2.5 \mu\text{m}$ using the optical and infrared spectrographs EFOSC2 and SofI at the ESO-NTT telescope (Buzzoni et al. 1984; Moorwood et al. 1998). The similar spectral resolution and the selection of comparable slit widths for both instruments ($R \sim 700$ -900 and slits widths of $0''.7$ and $0''.6$ for EFOSC2 and SOFI, respectively) allowed us to acquire optical and infrared spectra of homogeneous characteristics.

The EFOSC2 spectrum (hereafter “optical spectrum”) was acquired with grism 16 and roughly ranges from $0.6 \mu\text{m}$ to $1.0 \mu\text{m}$. The infrared SOFI spectra were taken using both the blue- (GB: $0.95 \mu\text{m}$ - $1.64 \mu\text{m}$) and red-grism (GR: $1.53 \mu\text{m}$ - $2.52 \mu\text{m}$). The optical and near-IR (NIR) data were acquired close in time on 12th and 16th February 2009, respectively. The total integration times on DK Cha were 300 s for the optical and 60 s and 20 s for the blue and red IR grism spectra. These were acquired through standard A-B nodding.

For data reduction standard IRAF¹ tasks were used. Wavelength calibrations were performed using argon-xenon

¹ IRAF (Image Reduction and Analysis Facility) is distributed by the National Optical Astronomy Observatories, which are operated

Table 1. Detected emission lines in DKCha.

Line id.	λ (μm)	EW (\AA)	F ($10^{-14} \text{ erg cm}^{-2} \text{ s}^{-1}$)	ΔF
[O I] $^1D_2-^3P_2$	0.630	-30.3	1.59	0.06
[O I] $^1D_2-^3P_1$	0.636	-19.4	0.83	0.10
H α	0.656	-135.8	9.28	0.18
[S II] $^2D_{5/2}-^4S_{3/2}$	0.672	-8.5	0.70	0.10
O I $^3P-^3S^{(m)}$	0.845	-17.9	5.44	0.47
Ca II $^2P_{3/2}-^2D_{3/2}$	0.850	-75.2	22.7	0.41
Ca II $^2P_{3/2}-^2D_{5/2}$	0.854	-53.9	16.9	0.01
Ca II $^2P_{1/2}-^2D_{3/2}$	0.866	-38.4	14.3	0.18
Pa 12	0.875	-8.1	3.04	0.22
[P I] $^2D^0-^4S^{(m)}$	0.879	-6.0	2.15	0.12
Pa δ	1.005	-8.2	4.65	0.42
N I $^4F_{3/2}-^4D_{3/2}^{(m)}$	1.013			
[S II] $^2P_{3/2}-^2D_{3/2}$	1.029	-3.4	2.21	0.37
[S II] $^2P_{1/2}-^2D_{3/2}$	1.034	-7.2	5.02	0.67
[N I] $^2P^0-^2D^{(m)}$	1.040	-3.6	2.80	0.39
[Ni II] $^4P_{5/2}-^2F_{7/2}$	1.046	-2.4	1.89	0.52
N I $^4D-^4P^{(m)}$	1.051	-2.8	2.32	0.60
N I $^4P-^4P^{(m)}$	1.062	-3.3	2.83	0.41
C I $^3D-^3P^{(m)}$	1.069	-10.5	10.2	0.35
C I $^3D_2-^3P_2^{(m)}$	1.073	-2.1	2.16	0.21
He I	1.083	-3.0	3.18	0.20
Pa γ	1.094	-11.6	12.6	1.33
O I $^3P-^3D^{(m)}$	1.129	-15.1	20.0	0.78
C I $^{(m)}$	1.175	-5.8	9.41	0.33
Ca II $^2P_{3/2}-^2S_{1/2}$	1.184	-7.7	12.8	0.67
[P II] $^3P_2-^1D_2$	1.188	-4.8	8.29	0.68
Ca II $^2P_{1/2}-^2S_{1/2}$	1.195	-1.9	3.37	0.37
Mg I $^1P^0-^1S_0$	1.198	-4.6	8.47	1.54
Mg I $^1P^0-^1D_2$	1.203	-3.5	6.39	0.11

Notes. (m) indicates lines belonging to multiplets. Observed fluxes, not corrected for extinction.

lamps. The NIR spectra were corrected for the atmospheric spectral response by dividing them by the spectrum of a suitable standard star. The three overlapping segments were then joined to obtain a single optical/IR spectrum of DK Cha. Unfortunately, during the two observing nights variable seeing conditions (seeing in the range of 0.75''-1.25'' and 1.0''-2.5'' for the optical and infrared data, respectively) prevented us from performing precise standard flux calibrations using spectro-photometric standards. This is because of considerable flux loss owing to the finite slit widths. To flux-calibrate the optical and infrared spectra we therefore employed the acquisition image (taken with the narrow-band filter NB 2.191) using four field stars as "standard stars". Moreover, additional photometric observations of DK Cha were acquired eight months later using the infrared spectrograph and camera ISAAC on the ESO-VLT telescope to test the goodness of the acquisition image photometry. The ISAAC narrow-band filter at 1.21 μm (where no significant spectral features were expected to contribute to the total flux) was chosen instead of the standard J broadband filter because of the bright J-magnitude of DK Cha (2MASS J~9.3 mag) that would otherwise saturate the detector. The photometric data and the acquisition image were reduced using standard IRAF¹ routines.

by AURA, Inc., cooperative agreement with the National Science Foundation.

Table 1. Continued.

Line id.	λ (μm)	EW (\AA)	F ($10^{-13} \text{ erg cm}^{-2} \text{ s}^{-1}$)	ΔF
Na I $^2P^0-^2S^{(m)}$	1.227	-1.9	0.39	0.03
[Fe II] $a^4D_{7/2}-a^6D_{9/2}^{(blend)}$	1.257	-1.1	0.27	0.02
C I $^3P^0-^3P^{(blend;m)}$	1.261	-0.5	0.12	0.04
Pa β	1.282	-16.9	4.43	0.09
Mg I $^1S^0-^1P_0^{(m)}$	1.488	-3.7	1.99	0.11
Mg I $^3P^0-^3S^{(m)}$	1.504	-10.5	5.67	0.33
Br 20	1.519	-3.0	1.65	0.20
Br 19	1.526	-1.5	0.84	0.24
Br 18	1.534	-1.9	1.09	0.19
Br 17	1.544	-2.0	1.14	0.30
Br 16	1.556	-3.1	1.84	0.11
Br 15	1.570	-2.7	2.02	0.12
Na I $^2S-^2P^{(m)}$	1.576	-4.1	2.65	0.25
Br 14	1.588	-7.7	5.04	0.25
[Fe II] $a^4D_{3/2}-a^4F_{7/2}$	1.600	-1.1	0.72	0.23
Br 13	1.611	-5.5	3.34	0.23
Br 12 $^{(blend)}$	1.641	-9.0	6.62	0.51
[Fe II] $a^4D_{7/2}-a^4F_{9/2}^{(blend)}$	1.644			
Br 11	1.681	-5.8	4.69	0.20
Na I $^2D-^2P^{(m)}$	1.689	-2.9	2.41	0.29
Mg I $^1P_1^0-^1S_0$	1.711	-2.0	1.77	0.20
Br 10 $^{(blendedwith?)}$	1.737	-7.7	8.35	0.66
H ₂ 1-0S(1)	2.122	-0.7	1.14	0.31
Br γ	2.166	-8.8	15.0	0.58
Na I $^2P_{3/2}^0-^2S_{1/2}^{(blend)}$	2.206	-2.2	3.87	0.54
Na I $^2P_{1/2}^0-^2S_{1/2}^{(blend)}$	2.209			
CO(2-0)	2.293	-0.6	1.17	0.24
CO(3-1)	2.323	-2.7	5.20	0.60
CO(4-2)	2.353	-2.2	4.33	0.64

Notes. (m) indicates lines belonging to multiplets. Observed fluxes, not corrected for extinction.

The magnitudes derived from both the ISAAC and acquisition image photometry agree within 0.1 mag, indicating no significant variations in the time elapsed between the observations.

3. Results

3.1. Detected lines

The optical and NIR spectra of DK Cha normalised to the stellar continuum are shown in Fig. 1. The spectra show numerous emission lines, most of them detected at S/N greater than 5, whereas no significant absorption features are detected. Line identification together with fluxes and equivalent widths are given in Table 1. Identification of these lines was made using the Atomic Line List database, while the goodness of the classification was checked through the detection of several transitions from the same atom and multiplet. In addition, the spectra of other YSOs (Kelly et al. 1994) and objects with expected similar excitation conditions (Walmsley et al. 2000) were also employed to recognise the features.

The DK Cha spectra show permitted emission lines similar to those observed in active YSOs, as for example the presence of H α , He I, the Ca II infrared triplet, and the Pa β and Br γ emission lines. Indeed, the most abundant features observed in our spectra are H I emission lines coming from the Brackett se-

Table 2. DK Cha photometry.

Filter	Magnitude
V	17.9
R _c	16.4
NB_1.21	10.5
H	7.9
K	6.0

rie. Permitted emission lines from species such as Na I, Mg I, C I, O I, and N I are also detected, showing upper state excitations above $30\,000\text{ cm}^{-1}$, $47\,000\text{ cm}^{-1}$, $69\,000\text{ cm}^{-1}$, $88\,000\text{ cm}^{-1}$ and $100\,000\text{ cm}^{-1}$, respectively. Several of these lines are usually observed in the optical and infrared spectra of CTTSs and low-mass Class I sources, as well as Herbig AeBe stars, while other lines (such as the N I lines) may be excited by fluorescence, which we will discuss in Sect. 4.3, and sometimes associated with photon dominated regions (PDRs; e.g. Marconi et al. 1998; Walmsley et al. 2000).

Forbidden emission lines such as [Fe II], [S II] and [O I] transitions are also detected in our spectra. These lines are commonly accepted to be associated with jets from young stars and are often observed in the spectra of low-mass CTTSs and Class I sources showing outflow activity (see, e.g. Hartigan et al. 1995; Nisini et al. 2005b; Podio et al. 2006).

Finally, in addition to the atomic lines, emission from molecular transitions are also observed in the infrared spectrum of DK Cha. In particular, weak H₂ emission at $2.12\text{ }\mu\text{m}$ and band-head CO emission around $2.3\text{ }\mu\text{m}$ have been detected.

3.2. Photometry

Table 2 shows the photometric value retrieved from the ISAAC photometry at $1.21\text{ }\mu\text{m}$ together with the V, R_c and K magnitudes derived from the measured fluxes in the DK Cha spectrum at each effective wavelength. As already mentioned, DK Cha is known to be a variable star. Hughes et al. (1991) and Molinari et al. (1993) studied the variability of DK Cha in a five-year period (from 1987 to 1992). They reported a ΔJ variability up to ~ 3 mag in 5 years. The K- and J-magnitudes reported in the literature vary between 5-6 mag and 9-11 mag (e.g., Alcalá et al. 2008; Hughes et al. 1991), respectively, while the V-magnitude ranges from V ~ 18.7 mag (Hughes et al. 1991) to V ~ 16.7 mag (Zacharias et al. 2004). Our measured magnitudes are within this range of values, indicating that at the time of the observations DK Cha was close to its brightness minimum.

4. Analysis and discussion

4.1. Extinction

Deriving the correct extinction value is crucial for the computation of YSO physical parameters. Frequently, extinction values are derived from colour excesses once a spectral type and an extinction law are assumed. The visual extinction (A_V) derived in this way depends on the adopted extinction law. Here, we have derived A_V from (I-R), (I-J) and (I-H) assuming the standard colours of Kenyon & Hartmann (1995) for a F0V star (Spezzi et al. 2008) and the reddening law of Cardelli et al. (1989) with $R_V=5.5$ because the interstellar medium in Chameleon clouds shows R_V values around 5-6 in the densest parts of the cloud (see, e.g. Covino et al. 1997; Spezzi et al. 2008). The discrepancies between the A_V val-

ues derived from different colours are not larger than ~ 2 mag ($A_V=10.4$ mag, 10.5 mag and 12.6 mag for the (I-R), (I-J) and (I-H) colours), with an average value of 11 ± 1 mag. For these estimates no veiling correction to the colours was considered. Nevertheless, ignoring the veiling will not lead to an A_V variation greater than 0.5 mag (see Cieza et al. 2005), which is within our A_V uncertainty of ± 1 mag. In addition, the derived A_V value agrees well with the extinction derived from the silicate absorption feature at $10\text{ }\mu\text{m}$ as detected in the ISO-SWS spectra by Acke & van den Ancker (2004). From their spectra of DK Cha, an A_V value ranging from ~ 10 mag to ~ 12 mag was derived, depending on whether the Rieke & Lebofsky (1985, $A_V/\tau(9.7)=16.6$) or the Mathis (1998, $A_V/\tau(9.7)=19.3$) relationships were used. In the following we adopt an average A_V value of 11 mag.

4.2. H I line emission

The line ratios among Brackett and Paschen lines can be used to obtain information on the physical conditions of the emitting gas, which helps us to determine the origin of the H I lines. The SOFI spectra taken with the blue- and red-grism allow us to simultaneously detect a series of Brackett lines from Br γ to Br 20, and the Paschen series lines Pa β , Pa γ and Pa δ . This allows us to minimise errors in the line ratios caused by line flux variability. In addition, line ratios are independent of uncertainties in the absolute flux calibration.

In Fig. 2 the ratios of the different Brackett and Paschen lines with respect to the Br γ and Pa β line (left and right panel, respectively) are shown as a function of their upper quantum number (n_{up}). Only unblended lines and those in clear atmospheric windows were taken into account. The fluxes of the lines were derived from the observed equivalent widths (EWs). Because DK Cha is of spectral type F0 (Spezzi et al. 2008), the contribution of the intrinsic photospheric component to the observed H I EWs cannot be neglected. Therefore, the EWs were corrected from the intrinsic photospheric absorption contribution following the same procedure as in Garcia Lopez et al. (2006). This procedure assumes that the observed flux is the sum of the emission from the stellar photosphere, the circumstellar gas and the disk. In addition, it assumes that the star dominates the V-band emission (see, Rodgers 2001). The latter assumption is furthermore supported by the fact that IMTTs are not veiled around 5500 \AA (Calvet et al. 2004). The EW of the photospheric component of each H I line, corrected for the H- and K-band veiling ($r_K \sim 0.6$, $r_H \sim 0.3$), was computed using a F0 spectral template from Rayner et al. (2009)². No veiling was detected in the J-band. All relevant parameters used to derive the photospheric equivalent widths as well as the stellar parameters are given in Tables 2 and 4. The equivalent widths of the circumstellar H I line components and the computed fluxes are shown in Table 3. The errors bars shown in Fig. 2 correspond to an uncertainty of $\pm 1\text{ \AA}$ in the EW_{circ} . In the same figure, the decrement observed in other YSOs is also plotted for comparison: namely, the line ratios as observed in the low-mass Class I source HH100-IRS (Podio et al. 2008; Nisini et al. 2005a) and the average values inferred from Bary et al. (2008) in a sample of CTTSs located in the Taurus cloud.

The DK Cha Brackett and Paschen ratios are very similar to those of low-mass CTTSs and Class I sources, although the T

² Online at the IRTF spectral library Web site: http://irtfweb.ifa.hawaii.edu/~spex/IRTF_Spectral_Library/Data.Format.html

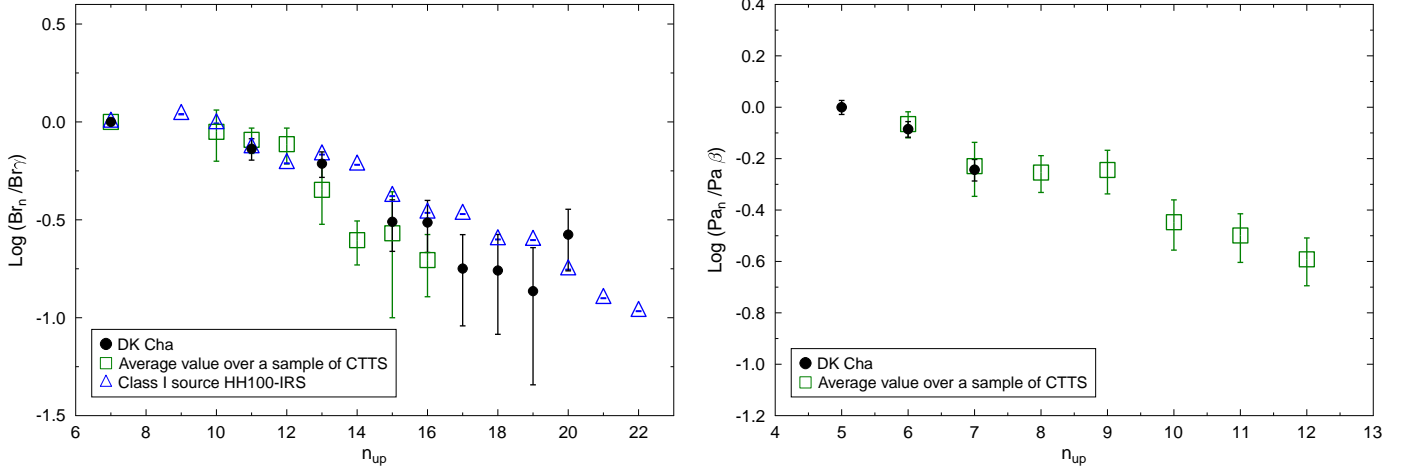


Fig. 2. **Left panel:** Ratio of the DK Cha Brackett lines with respect to $Br\gamma$ plotted as a function of the upper quantum number (n_{up} ; filled black circles). For comparison the Brackett decrements for the Class I source HH100-IRS (Nisini et al. 2004, open blue triangles) and the weighted mean line ratios for the Brackett series on the CTTSs sample of Bary et al. (2008, open green squares) are also included in the plot. **Right panel:** Ratio of the DK Cha Paschen lines with respect to the $Pa\beta$ line as a function of the upper quantum number n_{up} (black filled circles). For comparison, the weighted mean line ratios for the Paschen series on the CTTSs sample of Bary et al. (2008, open green squares) are also shown.

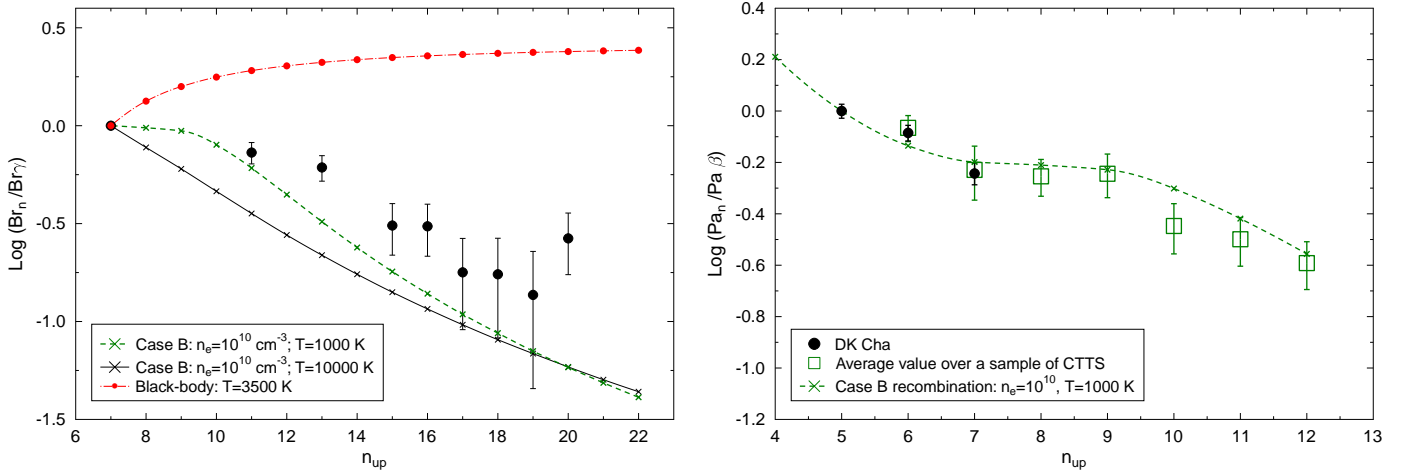


Fig. 3. **Left panel:** Comparison between the observed DK Cha Brackett decrement and the expected curves for Case B recombination and black-body emission. The crosses represent the ratios from case B recombination at $T=10\,000 \text{ K}$, $n=10^{10} \text{ cm}^{-3}$ (black continuous line) and $T=1000 \text{ K}$, $n=10^{10} \text{ cm}^{-3}$ (green dashed line), while dots represent the black-body curves at $T=3500 \text{ K}$ (dashed red line). **Right panel:** Comparison between the observed DK Cha Paschen decrement (black dots), the Paschen decrement of the CTTSs sample of Bary et al. (2008, open green squares) and the expected Paschen ratios from Case B recombination at $T=1000 \text{ K}$, $n=10^{10} \text{ cm}^{-3}$ (green dashed line).

Tauri sample of Bary et al. (2008) have slightly lower Brackett ratios at $N_{up} > 13$ with respect to DK Cha and HH100IRS. This might indicate that the excitation conditions giving rise to the Brackett series have a weak dependence on the mass and evolutionary stage of the source.

4.2.1. Case B recombination

To constrain the physical conditions where the Brackett and Paschen lines originate, we have explored different excitation mechanisms. In particular, Bary et al. (2008) found that the Brackett and Paschen decrements of their sample of CTTSs

were always fairly well fitted by a standard Case B recombination at low gas temperature ($\lesssim 2000 \text{ K}$). In Fig. 3 we plot the expected ratios under Case B conditions that fit the Bary's sample ($n=10^{10} \text{ cm}^{-3}$, and $T=1000 \text{ K}$), derived from the Hummer & Storey (1987) calculations³. We find that this model is unable to reproduce the observed Brackett decrement in DK Cha, because the line ratios at $N_{up} \gtrsim 12$ are all underestimated. Better fits in the Case B regime are not obtained even if we

³ To derive the Case B predictions, the Fortran program provided by Storey & Hummer (1995) and the required data files available at <http://vizier.u-strasbg.fr/viz-bin/VizieR?source=VI/64>, have been used.

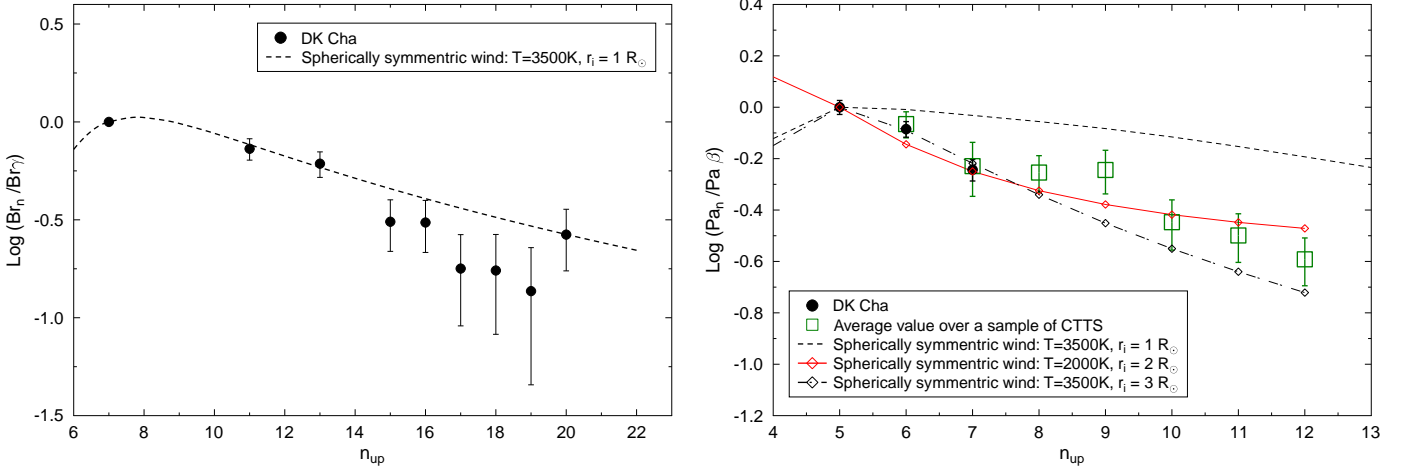


Fig. 4. **Left panel:** Comparison between the DK Cha Brackett decrement and a model assuming an expanding wind in LTE at $T=3500\text{K}$. The other parameters of the model are: $r_i=1 R_\odot$, $r_{out}=5 R_\odot$, $n_e^{ini}=10^{13}\text{cm}^{-3}$, $V_0=20\text{km s}^{-1}$, $V_{max}=300\text{km s}^{-1}$ and $\alpha=3$ (see text for details). **Right panel:** Comparison between the DK Cha Paschen decrement and the same model assuming an expanding wind in LTE at $T=3500\text{K}$ and $r_i=3 R_\odot$ (dashed-dot black line) and at $T=2000\text{K}$ and $r_i=2 R_\odot$ (continuous red line). The other model parameters are the same as in the Brackett decrement case. For comparison the weighted mean line ratios for the Paschen series on the CTTSs sample of Bary et al. (2008, open green squares) were also included.

Table 3. Brackett and Paschen line fluxes.

Line	EW_{circ}^a (\AA)	F^b ($10^{-12}\text{erg s}^{-1}\text{cm}^{-2}$)
Pa δ	-12.9	9.33
Pa γ	-18.6	13.4
Pa β	-23.0	16.3
Br 20	-3.0	2.04
Br 19	-1.5	1.02
Br 18	-1.9	1.30
Br 17	-2.0	1.33
Br 16	-3.4	2.29
Br 15	-3.4	2.31
Br 13	-6.7	4.56
Br 11	-8.0	5.44
Bry	-11.2	7.46

^a Equivalent width of the circumstellar H I line. Uncertainties are estimated to be $\pm 1\text{\AA}$.

^b Fluxes corrected by an extinction of $A_V=11\text{mag}$

increase the possible range of electron densities and temperatures: this suggests that the different behaviour of the Brackett lines in DK Cha with respect to the Bary et al. (2008) sample of CTTSs is not caused by the higher luminosity/mass of the source. Unfortunately, we cannot prove which the behaviour of the Paschen lines at higher n_{up} is, because only the Pa β Pa γ and Pa δ lines were detected at a sufficiently high S/N in a clear atmospheric region and not blended with other emission lines.

Evidence that the H I lines in DK Cha cannot be reproduced by the optically thin regime assumed in the Case B recombination is also provided by the observed (extinction corrected) Pa β /Bry ratio. This ratio is 2.18 ± 0.04 , while for Case B it is never below 2.5: indeed, very low values of Pa β /Bry are obtained only when the two lines are optically thick in LTE at low temperatures (Gatti et al. 2006; Antonucci et al. 2011). An estimate of the temperature and projected emitting area that gives rise to

this thick emission can be obtained from the Pa β /Bry ratio and the Pa β flux. Assuming a line-width of 150km s^{-1} , we derive $T\sim 3500\text{K}$ and a projected area of the order of a few solar radii. This indicates that the emission originates from a quite compact region with gas at low temperature. To verify the consistency of our previous statement, we also plot in Fig. 3 (left panel) the expected Brackett decrement for a black-body at $T=3500\text{K}$ (red dotted dashed line), i.e., assuming that all Brackett lines are optically thick and at the same temperature. Evidently, the predicted high- n_{up} lines are largely overestimated with respect to the Bry. Summarising this analysis, we conclude that the DK Cha Brackett decrement is consistent with emission at a quite low temperature where the lines are optically thick for the transitions at low n_{up} and optically thin for the higher n_{up} values. On the other hand, no additional information can be retrieved from our Paschen decrement (Fig. 3, right panel).

As discussed by Bary et al. (2008), the low temperature derived for the excitation of the Brackett and Paschen lines is not consistent with an origin in magneto-spheric accretion columns, where the temperatures are predicted to be in the range 6000-12000 K (Muzerolle et al. 1998a). Bary et al. (2008) suggested that the direct absorption of high energy photons from the hot corona and/or accretion shock is potentially able to ionise the gas and produce the intense H I emission even at low temperatures. Qualitatively this seems applicable to the DK Cha case, which is a well known X-ray source with an X-ray luminosity of $L_X\sim 1.3\times 10^{31}\text{erg s}^{-1}$ (Hamaguchi et al. 2005).

4.2.2. Spherically symmetric expanding wind model

Finally, to explore a different excitation scenario, we also compared the observed Brackett and Paschen decrements with the predictions of a simple model of an expanding wind, which was able to consistently reproduce the H I line emission in the Class I source HH100-IRS (Nisini et al. 2004). This model consists of a spherical envelope of ionised hydrogen in LTE, where the gas is expanding from an inner radius r_i to an outer radius r_{out} following a velocity law of the type $V(r)=V_0+(V_{max}-V_0)(1-(r_i/r)^\alpha)$,

where V_0 is the initial velocity at the base of the wind and V_{max} is the maximum velocity of the wind (see Nisini et al. 2004, 1995, for more details). Under these conditions, the line decrement mainly depends on the optical depth of the line, which is influenced by the velocity law, the emitting region size, and the electron density assumed at the wind base. Assuming a $T \sim 3500$ K and an emitting region size with radius $\sim 5 R_\odot$, we are able to find quite a good agreement with all observed Brackett line ratios with a model having a $V_{max} \sim 300 \text{ km s}^{-1}$ and $n_e^{ini} \sim 10^{13} \text{ cm}^{-3}$ (Fig. 4, left panel). This model is also able to reproduce the $\text{Pa}\beta/\text{Br}\gamma$ ratio as well as the extinction-corrected $\text{Pa}\beta$ flux of $\sim 1 \times 10^{-11} \text{ erg cm}^{-2} \text{ s}^{-1}$.

We point out that although this is a toy model, the main results do not depend much on the given assumptions. Although the main approximation here is spherical geometry, the high gas speed and the consequent high velocity gradients imply that the radiative interaction occurs only in the confined region of line formation. Consequently, the line emissivity depends only on local physical quantities and line ratios are not much affected by geometrical effects.

The assumption of spherical wind is instead affecting the mass loss rate implied by our model: indeed, an estimate of \dot{M}_w can be given from the continuity equation:

$$\dot{M}_w = 4\pi r_i^2 V_0 n_e^{ini} \quad (1)$$

Substituting the relevant parameters, we derive $\dot{M}_w = 3.0 \times 10^{-7} M_\odot \text{ yr}^{-1}$. Such a value is of the same order of magnitude as the DK Cha mass accretion rate derived in Sect. 4.4. However, \dot{M}_w (eq. 1) scales with the total surface area and could be a small fraction of the derived value if the emission comes, e.g., from a collimated wind.

It is also worth noting that the same wind parameters used to fit the Brackett ratios do not reproduce the Paschen decrement, however (see, Fig. 4, right panel; black dashed line). Lower temperatures ($T \sim 2000$ K) or a greater envelope thickness (around a factor of 2-3) are required to match the previous wind solution. This may indicate that Paschen lines are emitted in a region that is more extended than the Brackett lines and/or that a temperature gradient is required. However, our model is probably too simplistic to draw further conclusions.

Kwan & Fischer (2011) performed local excitation calculations to obtain hydrogen line opacities and emissivity ratios, finding out that the H I line emission mainly arises from a highly clumpy radial outflow. Following this work, the observed $\text{Pa}\gamma/\text{Pa}\beta$ ratio in DK Cha ($\text{Pa}\gamma/\text{Pa}\beta = 0.82 \pm 0.07$) is consistent with $\text{Pa}\beta$ and $\text{Pa}\gamma$ lines excited in a region with a total density of roughly $N_H \sim 1.6 \times 10^{11} - 6 \times 10^{11} \text{ cm}^{-3}$ and an optical depth $\tau_{\text{Pa}\gamma} = 33.4 - 210$, with both lines showing different excitation temperatures in the range 3240-3920 K and 3020-3940 K, respectively. This result resembles that from our simple model fairly well.

4.3. Other detected lines.

Previous observations of DK Cha have already shown some of the properties of its circumstellar material. For instance, Hughes et al. (1991) reported the presence of a wind from this source as shown by blue-shifted forbidden line emission, whereas van Kempen et al. (2009) detected a CO outflow. In our spectra, the presence of faint H_2 emission together with the CO band-heads may also indicate the presence of a molecular outflow. However, the near-IR H_2 and CO emission could also be

related to emission from the interaction of a wind with the surrounding medium (e.g., Garcia Lopez et al. 2008) or/and emission from the inner warm circumstellar disk (Carr et al. 1993; Najita et al. 1996).

The optical and NIR spectrum shows several forbidden emission lines that are typical of atomic jets, such as the several [S II] [O I] and [N I] transitions between 0.6 and $1 \mu\text{m}$. The presence of a jet from DK Cha was already pointed out by Hughes et al. (1991), who resolved [S II] extended emission showing significant velocity gradients. From the luminosity of the [O I] $0.630 \mu\text{m}$ it is possible to estimate the mass flux rate from the jet (\dot{M}_{jet}), following the relationship given by Hartigan et al. (1995). The main uncertainty using this expression is caused by the assumed extinction: the A_V derived in Sect. 4.1 towards the central source can be considered an upper limit to the extinction towards the region of the emission of the forbidden lines, which is likely to be located farther out in a less embedded environment. Therefore, we can only give an upper limit to the mass flux by assuming $A_V = 11$ mag for the extinction towards the forbidden line emission region. In this way, we infer that \dot{M}_{jet} is $\lesssim 10^{-6} M_\odot \text{ yr}^{-1}$, assuming a distance to the source of ~ 178 pc, an electron density of $\sim 10^5 \text{ cm}^{-3}$ (because both emission from [O I] and [S II] have been detected, see Hartigan et al. 1995), and a velocity in the plane of the sky $V_\perp \sim 32 \text{ km s}^{-1}$ (assuming $i \sim 18^\circ$ and a radial velocity of $\sim -98 \text{ km s}^{-1}$; van Kempen et al. 2010; Hughes et al. 1991). To better constrain the \dot{M}_{jet} value in DK Cha, the [O I] $63 \mu\text{m}$ line has been used as well. This line has been detected in both ISO-LWS and HERSCHEL-PACS observations of DK Cha (van Kempen et al. 2010; Lorenzetti et al. 1999). Although this line is not affected by extinction, the \dot{M}_{jet} value derived from it represents an upper limit to the total mass transported along the jet because part of the [O I] $63 \mu\text{m}$ line could be excited in the PDR of the star (see e.g., Lorenzetti et al. 1999). Assuming a [O I] $63 \mu\text{m}$ line flux of $3.7 \times 10^{-12} \text{ erg s}^{-1} \text{ cm}^{-2}$ (van Kempen et al. 2010) and the expression reported in Cabrit (2002) to estimate \dot{M}_{jet} , we found an upper limit of $\sim 3.6 \times 10^{-7} M_\odot \text{ yr}^{-1}$.

HERSCHEL-PACS observations of this source also revealed the presence of several H_2O and OH lines interpreted as possibly generated from UV-heating of the material along the cavity walls and thus pointing out the presence of a strong UV field from the protostar (van Kempen et al. 2010). The optical and NIR spectra of DK Cha presented in this work show, indeed, several permitted transitions that are likely excited by UV pumping. The O I $0.845 \mu\text{m}$ and O I $1.129 \mu\text{m}$ lines are two good examples: the presence of the bright O I $1.129 \mu\text{m}$ emission together with the absence of the O I $1.132 \mu\text{m}$ line indicate H I Ly β fluorescence of the $3d^3D$ level of O I as the pumping mechanism for the O I $0.845 \mu\text{m}$ line. This suggests in turn that the H α line must be optically thick in this source because a large population of the $n=3$ level of hydrogen is needed for this process to occur (Grandi 1975, 1980). Oxygen I fluorescence lines have been reported before in other Herbig Ae/Be stars, as MWC 349 and R Mon (see e.g. Kelly et al. 1994). In addition to the O I lines, several N I transitions at 1.013, 1.051 and $1.060 \mu\text{m}$, which may be also excited by fluorescence, have been observed. Walmsley et al. (2000) have already reported the presence of some of these lines in the spectrum of the Orion bar. They attributed the excitation of these lines to fluorescence within the ionisation front.

4.4. Accretion luminosity and mass accretion rate.

The accretion luminosity (L_{acc}) in embedded YSOs is mostly derived from the luminosity of infrared lines such as the Br γ and Pa β lines (Muzerolle et al. 1998b). The Br γ line has been successfully used to derive the accretion luminosity in objects ranging from brown-dwarfs to several solar masses (Calvet et al. 2004; Garcia Lopez et al. 2006), however, the Pa β line has been mostly used to compute the accretion luminosity in low-mass protostars (Gatti et al. 2008; Natta et al. 2006). The simultaneous acquisition of the SOFI blue and red grism spectra allows us to derive L_{acc} from the luminosity of the Pa β and Br γ lines, which gives us the opportunity of comparing the inferred L_{acc} values without introducing any uncertainty caused by intrinsic flux line variations of the source.

With this aim, the empirical relations relating the accretion luminosity with the Br γ and Pa β luminosity (Calvet et al. 2004 and Calvet et al. 2000) were used:

$$\log L_{acc}/L_{\odot} = 2.9 + 0.9 \log L(Br\gamma) \quad (2)$$

$$\log L_{acc}/L_{\odot} = 2.80 + 1.03 \log L(Pa\beta). \quad (3)$$

The luminosities of the Br γ and Pa β lines ($L(Br\gamma)$, $L(Pa\beta)$) were derived from the observed equivalent widths of the Br γ and Pa β lines ($EW(Br\gamma)$, $EW(Pa\beta)$) once they were corrected from the intrinsic photospheric absorption contribution (see Sect.4.2).

Using this procedure, we found a very good agreement between the accretion luminosity computed from the Br γ and Pa β luminosities (see, Table 5), with an average value of $L_{acc} \sim 9 L_{\odot}$.

Additional relationships, based on the luminosity of optical lines, have also been suggested for the determination of the accretion luminosity. For instance, Herczeg & Hillenbrand (2008), Dahm (2008) and Fang et al. (2009), derived relationships based on the luminosity of the [O I], Ca II and H α lines, respectively. When we apply these relationships to the lines observed in DK Cha, we derive accretion luminosities much higher than the value estimated from the IR H I lines, however ($L_{acc} \sim 104$, 24 and 107 L_{\odot} for the [O I], Ca II and H α lines, respectively), and, more important, much higher than the bolometric luminosity of this source. The origin of this discrepancy could be related to a wrong extinction estimate. For instance, decreasing the A_V of 2 mag, new L_{acc} values of ~ 7.4 , 4.5, 11.7, 18.6 and 12 L_{\odot} are found for the Br γ , Pa β , Ca II, O I and H α , respectively. Although these values are now lower than L_{bol} , the accretion luminosities derived from the Br γ and Pa β lines now disagree. Similar results to the ones found in DK Cha (i.e. optical lines giving rise to L_{acc} values higher than IR lines) have also been reported in a large sample of sources showing low extinction values located in the ChI/II clouds (Antoniucci et al. 2011).

It is more likely, then, that the empirical relationships found for samples of low or very low mass objects cannot be extrapolated to sources with larger mass and luminosity. In the high-luminosity objects different excitation mechanisms in addition to accretion can indeed be responsible for enhanced emission of the optical lines such as high chromosphere activity or direct excitation from stellar UV photons.

From the accretion luminosity derived from the IR lines and stellar parameters shown in Table 4 a mass accretion rate (\dot{M}_{acc}) of $\sim 3.5 \times 10^{-7} M_{\odot} \text{ yr}^{-1}$ was found from the expression (Gullbring et al. 1998)

$$\dot{M}_{acc} = \frac{L_{acc} R_*}{GM_*} \left(1 - \frac{R_*}{R_{in}} \right)^{-1}, \quad (4)$$

Table 4. DKCha stellar parameters.

ST	D	T_{eff}	L_*	L_{bol}	R_*	M_*
	(pc)	(K)	(L_{\odot})	(L_{\odot})	(R_{\odot})	(M_{\odot})
F0 ^a	178	7200 ^a	18.62 ^a	29.4 ^b	2.77 ^a	2 ^a

^a From Spezzi et al. (2008)

^b From van Kempen et al. (2010)

Table 5. Accretion properties.

A_V	$L_{acc}(Pa\beta)$	$L_{acc}(Br\gamma)$	\dot{M}_{acc}
(mag)	(L_{\odot})	(L_{\odot})	($10^{-7} M_{\odot} \text{ yr}^{-1}$)
11.2	9.5	9.1	3.5

where R_* and M_* are the stellar radius and mass, G is the universal constant and a $R_{in}=5 R_{\odot}$ is the inner disk radius. The inferred \dot{M}_{acc} value is within the range of those found in classical Herbig Ae stars and intermediate mass T Tauri stars (IMTTS) where \dot{M}_{acc} in the range 10^{-6} - $10^{-8} M_{\odot} \text{ yr}^{-1}$ are typically found (Donehew & Brittain 2011; Garcia Lopez et al. 2006; Calvet et al. 2004; Rodgers 2001). Interestingly, when one compares sources of roughly the same mass, the \dot{M}_{acc} value found in DK Cha is higher than that found in the IMTTS sample of Calvet et al. (2004) and in Garcia Lopez et al. (2006) (where \dot{M}_{acc} values $\sim 10^{-8} M_{\odot} \text{ yr}^{-1}$ were found) but lower than that computed for the Class I sample of White & Hillenbrand (2004) ($\dot{M}_{acc} \sim 10^{-6} M_{\odot} \text{ yr}^{-1}$). This result is consistent with DK Cha being in an evolutionary transition phase between a Class I and II source.

5. Conclusions

We have presented low-resolution spectroscopic observations of the embedded Herbig Ae star DK Cha covering the range $0.6 \mu\text{m}$ - $2.4 \mu\text{m}$. Its nearly face-on configuration has allowed us to have direct access to the star-disk system and to detect numerous emission lines tracing different emission regions and excitation conditions in the nearby surroundings of the protostar. The extremely rich emission line spectrum makes this source very similar to low-mass very active T Tauri stars. We summarise our results as follows:

- The DK Cha spectrum shows several permitted (e.g., Ca II, Mg I, Na I), forbidden (e.g., [Fe II], [S II]) and molecular emission lines (CO and H₂). The H I lines are those more numerous along the spectrum. In addition, some of the permitted lines, such as the O I 0.845 μm line, were identified as being excited by fluorescence.
- To constrain the origin of the H I lines, Brackett decrement plots were constructed and compared with different excitation mechanisms. Case B recombination is not able to fit all observed Brackett ratios, while optically thick emission in LTE at a temperature of ~ 3500 K is required to account for the observed Pa β /Br γ ratio. A simple model for an expanding gas is able to reproduce all observed Brackett ratios by assuming that this gas is located very close to the central source and has a high density at its base, of the order of 10^{13} cm^{-3} . The same parameters used to reproduce the Brackett ratios cannot account for the Paschen line ratios.
- From the Pa β and Br γ line luminosity we derived the accretion luminosity using the expressions from Calvet et al.

(2000, 2004). We found a very good agreement between the L_{acc} derived from both expressions, with an average value of $L_{acc} \sim 9L_{\odot}$. From the accretion luminosity a $\dot{M}_{acc} \sim 3.5 \times 10^{-7} M_{\odot} \text{yr}^{-1}$ was found. The measured \dot{M}_{acc} value is consistent with DK Cha being in an evolutionary transition phase between a Class I and II source.

Acknowledgements. The authors kindly thanks the following people (in alphabetical order) who contributed to the Atomic Line List v2.05b12 (<http://www.pa.uky.edu/~peter/atomic/>) by providing data and/or helpful insights: K.M. Aggarwal, M.A. Bautista, R. Kisielius, S.N. Nahar, M.J. Seaton, D.A. Verner. We are grateful to Malcolm Walmsley and Antonella Natta for fruitful discussions and insightful comments. RGL, ACG and TR were supported by the Science Foundation Ireland, grant 07/RFP/PHYF790. ACG also acknowledges support from the European Commission, grant ERG249157.

References

- Acke, B. & van den Ancker, M. E. 2004, A&A, 426, 151
 Alcalá, J. M., Spezzi, L., Chapman, N., et al. 2008, ApJ, 676, 427
 Antonucci, S., Garcia Lopez, R., Nisini, B., et al. 2011, ArXiv e-prints; arXiv:1108.2622
 Bary, J. S., Matt, S. P., Skrutskie, M. F., et al. 2008, ApJ, 687, 376
 Buzzoni, B., Delabre, B., Dekker, H., et al. 1984, The Messenger, 38, 9
 Cabrit, S. 2002, in EAS Publications Series, Vol. 3, EAS Publications Series, ed. J. Bouvier & J.-P. Zahn, 147–182
 Calvet, N., Hartmann, L., & Strom, S. E. 2000, Protostars and Planets IV, 377
 Calvet, N., Muzerolle, J., Briceño, C., et al. 2004, AJ, 128, 1294
 Caratti o Garatti, A., Garcia Lopez, R., Antonucci, S., et al. 2011, A&A, submitted
 Cardelli, J. A., Clayton, G. C., & Mathis, J. S. 1989, ApJ, 345, 245
 Carr, J. S., Tokunaga, A. T., Najita, J., Shu, F. H., & Glassgold, A. E. 1993, ApJ, 411, L37
 Cieza, L. A., Kessler-Silacci, J. E., Jaffe, D. T., Harvey, P. M., & Evans, II, N. J. 2005, ApJ, 635, 422
 Covino, E., Palazzi, E., Penprase, B. E., Schwarz, H. E., & Terranegra, L. 1997, A&AS, 122, 95
 Dahm, S. E. 2008, AJ, 136, 521
 Donehew, B. & Brittain, S. 2011, AJ, 141, 46
 Fang, M., van Boekel, R., Wang, W., et al. 2009, A&A, 504, 461
 Garcia Lopez, R., Natta, A., Testi, L., & Habart, E. 2006, A&A, 459, 837
 Garcia Lopez, R., Nisini, B., Giannini, T., et al. 2008, A&A, 487, 1019
 Gatti, T., Natta, A., Randich, S., Testi, L., & Sacco, G. 2008, A&A, 481, 423
 Gatti, T., Testi, L., Natta, A., Randich, S., & Muzerolle, J. 2006, A&A, 460, 547
 Giannini, T., Lorenzetti, D., Tommasi, E., et al. 1999, A&A, 346, 617
 Grandi, S. A. 1975, ApJ, 196, 465
 Grandi, S. A. 1980, ApJ, 238, 10
 Gullbring, E., Hartmann, L., Briceno, C., & Calvet, N. 1998, ApJ, 492, 323
 Hamaguchi, K., Yamauchi, S., & Koyama, K. 2005, ApJ, 618, 360
 Hartigan, P., Edwards, S., & Ghandour, L. 1995, ApJ, 452, 736
 Herczeg, G. J. & Hillenbrand, L. A. 2008, ApJ, 681, 594
 Hughes, J. D., Hartigan, P., Graham, J. A., Emerson, J. P., & Marang, F. 1991, AJ, 101, 1013
 Hummer, D. G. & Storey, P. J. 1987, MNRAS, 224, 801
 Kelly, D. M., Rieke, G. H., & Campbell, B. 1994, ApJ, 425, 231
 Kenyon, S. J. & Hartmann, L. 1995, ApJS, 101, 117
 Kwan, J. & Fischer, W. 2011, MNRAS, 411, 2383
 Lorenzetti, D., Tommasi, E., Giannini, T., et al. 1999, A&A, 346, 604
 Marconi, A., Testi, L., Natta, A., & Walmsley, C. M. 1998, A&A, 330, 696
 Mathis, J. S. 1998, ApJ, 497, 824
 Molinari, S., Liseau, R., & Lorenzetti, D. 1993, A&AS, 101, 59
 Moorwood, A., Cuby, J., & Lidman, C. 1998, The Messenger, 91, 9
 Muzerolle, J., Calvet, N., & Hartmann, L. 1998a, ApJ, 492, 743
 Muzerolle, J., Hartmann, L., & Calvet, N. 1998b, AJ, 116, 2965
 Najita, J., Carr, J. S., Glassgold, A. E., Shu, F. H., & Tokunaga, A. T. 1996, ApJ, 462, 919
 Natta, A., Testi, L., & Randich, S. 2006, A&A, 452, 245
 Nisini, B., Antonucci, S., & Giannini, T. 2004, A&A, 421, 187
 Nisini, B., Antonucci, S., Giannini, T., & Lorenzetti, D. 2005a, A&A, 429, 543
 Nisini, B., Bacciotti, F., Giannini, T., et al. 2005b, A&A, 441, 159 (N05)
 Nisini, B., Milillo, A., Saraceno, P., & Vitali, F. 1995, A&A, 302, 169
 Podio, L., Bacciotti, F., Nisini, B., et al. 2006, A&A, 456, 189 (P06)
 Podio, L., Garcia, P. J. V., Bacciotti, F., et al. 2008, A&A, 480, 421
 Rayner, J. T., Cushing, M. C., & Vacca, W. D. 2009, ApJS, 185, 289
 Rieke, G. H. & Lebofsky, M. J. 1985, ApJ, 288, 618
 Rodgers, B. M. 2001, PhD thesis, UNIVERSITY OF WASHINGTON
 Spezzi, L., Alcalá, J. M., Covino, E., et al. 2008, ApJ, 680, 1295
 Storey, P. J. & Hummer, D. G. 1995, VizieR Online Data Catalog, 6064, 0
 van Kempen, T. A., Green, J. D., Evans, N. J., et al. 2010, A&A, 518, L128+
 van Kempen, T. A., Hogerheijde, M. R., van Dishoeck, E. F., et al. 2006, A&A, 454, L75
 van Kempen, T. A., van Dishoeck, E. F., Hogerheijde, M. R., & Güsten, R. 2009, A&A, 508, 259
 Walmsley, C. M., Natta, A., Oliva, E., & Testi, L. 2000, A&A, 364, 301
 White, R. J. & Hillenbrand, L. A. 2004, ApJ, 616, 998
 Zacharias, N., Monet, D. G., Levine, S. E., et al. 2004, in Bulletin of the American Astronomical Society, Vol. 36, Bulletin of the American Astronomical Society, 1418–+